with the boundary conditions for $Y(\xi)$ given by

$$Y(0)=Y'(0)=Y''(1)=Y'''(1)=0$$

Substituting the solution (7) into Eq. (6), the following nonlinear algebraic equation is obtained:

$$k^4+2\omega^2(1+\cosh\lambda_2\cos\lambda_1)-2\omega k^2\sinh\lambda_2\sin\lambda_1=0 \qquad (8)$$

where

$$\lambda_1=[(\omega^2+k^4/4)^{1/2}-k^2/2]^{1/2}$$

and

$$\lambda_2=[(\omega^2+k^4/4)^{1/2}+k^2/2]^{1/2}$$

Equation (8) is a nonlinear algebraic equation for the solution of the natural frequency ω. For a given value of k^2, Eq. (8) will yield a family of values of ω's corresponding to the various natural frequencies. This is seen to be an equation with multiple solutions where all the solutions are physically meaningful. Anderson and King[3] gave the first three natural frequencies in their work. We will now apply the method of parameter differentiation to systematically search for the multiple solutions.

The differential equation corresponding to Eq. (3) for the solution of Eq. (8) is

$$\left\{4\omega(1+\cosh\lambda_2\cos\lambda_1)-k^2\sinh\lambda_2\sin\lambda_1+\frac{\omega^2}{(\omega^2+k^4/4)^{1/2}}\left[\frac{\sinh\lambda_2\cos\lambda_1}{\lambda_2}-\frac{\cosh\lambda_2\sin\lambda_1}{\lambda_1}\right]-\frac{\omega^2k^2}{2(\omega^2+k^4/4)^{1/2}}\left[\frac{\cosh\lambda_2\sin\lambda_1}{\lambda_2}+\frac{\sinh\lambda_2\cos\lambda_1}{\lambda_1}\right]\right\}\frac{d\omega}{d\tau}$$
$$=-[k^4+2\omega_0^2(1+\cosh\lambda_{20}\cos\lambda_{10})-\omega_0k^2\sinh\lambda_{20}\sin\lambda_{10}] \qquad (9)$$

Table 1 Solutions of $\omega(\tau)$ for various values of ω_0 ($k^2=20$)

$\omega=1$		$\omega=5$		$\omega=10$	
τ	$\omega(\tau)$	τ	$\omega(\tau)$	τ	$\omega(\tau)$
0.0	1.0000	0.0	5.0000	0.0	10.0000
0.2	1.2409	0.2	4.5996	0.2	9.2058
0.4	1.4405	0.4	4.1398	0.4	8.2707
0.6	1.6141	0.6	3.5934	0.6	7.1022
0.8	1.7695	0.8	2.9047	0.8	5.4592
1.0	1.9112	1.0	1.9112	1.0	1.9112
$\omega=25$		$\omega=40$		$\omega=50$	
τ	$\omega(\tau)$	τ	$\omega(\tau)$	τ	$\omega(\tau)$
0.0	25.000	0.0	40.000	0.0	50.000
0.2	25.583	0.2	38.626	0.2	47.432
0.4	26.066	0.4	37.030	0.4	44.697
0.6	26.483	0.6	35.070	0.6	41.516
0.8	26.853	0.8	32.392	0.8	37.250
1.0	27.187	1.0	27.184	1.0	27.182
$\omega=67$		$\omega=80$		$\omega=100$	
τ	$\omega(\tau)$	τ	$\omega(\tau)$	τ	$\omega(\tau)$
0.0	67.000	0.0	80.000	0.0	100.000
0.2	67.387	0.2	78.572	0.2	96.455
0.4	67.749	0.4	76.929	0.4	92.605
0.6	68.089	0.6	74.964	0.6	88.079
0.8	68.410	0.8	72.451	0.8	81.996
1.0	68.716	1.0	68.714	1.0	68.712

where

$$\lambda_{10}=[(\omega_0^2+k^4/4)^{1/2}-k^2/2]^{1/2}$$

$$\lambda_{20}=[(\omega_0^2+k^4/4)^{1/2}+k^2/2]^{1/2}$$

and the initial condition is

$$\tau=0: \quad \omega(0)=\omega_0$$

Equation (9) is integrated by using Runge-Kutta method with $\Delta\tau=0.005$. To illustrate the procedure, let us consider the case in which $k^2=20$. By assigning ω_0 equal to $n\Delta\omega_0$, where n is taken to be 1,2, 3,..., successively, the solutions will naturally approach the individual natural frequencies, as demonstrated in Table 1. The first three cases in Table 1 ($\omega_0=1,5,10$) lead to the same natural frequency, $\omega=1.911$, even though their initial assumptions are different. Similar comments can be made relative to the other six cases. Namely, case 4-6 all approach to $\omega=27.18$ and cases 7-9 all approach to $\omega=68.71$, respectively. If higher natural frequencies are required, we simply continue to process by systemmatically using the values of ω_0 and the solutions of Eq. (9) at $\tau=1$ will naturally approach to the various natural frequencies.

References

[1] Kane, T. R., "Real Solutions of Sets of Nonlinear Equations," *AIAA Journal*, Vol. 4, Oct. 1966, pp. 1880-1881.

[2] Yakolev, M. N., "Solutions of Systems of Nonlinear Equations by a Method of Differentiation With Respect to a Parameter," *USSR Computational Mathematics*, Vol. 4, Jan. 1964, pp. 198-203.

[3] Anderson, J. M. and King, W. M., "Vibration of a Cantilever Subject to a Tensile Follower Force," *AIAA Journal*, Vol. 7, April 1969, pp. 741-742.

Experiment for Evaluation of Acceleration Measurement Capability

D. K. Overmier* and M. J. Forrestal†
Sandia Laboratories, Albuquerque, N. Mex.

DEVELOPMENT and qualification tests subjecting re-entry vehicles to impulse loads usually include measurements of acceleration response of internal components. Prior to testing, analytical predictions are made of the component responses to be measured. In general, complexity of structure and difficulties in representing load paths to components lead to analytical results of low credibility. In typical full-scale tests, records show negligible resemblance to the predictions, and frequently appear hopelessly contaminated with mechanical or electrical noise. The analyst and the component designer find themselves in the predicament of trying to establish component design or test criteria by reconciling predictions and test data in which they possess little faith.

To estimate a confidence level for certain component acceleration measurements, some experiments were performed using a simple structure having predictable response. The simple structure chosen was an aluminum ring comparable in structural response behavior to a vehicle cross section. A

Received January 20, 1975. This work was supported by the U. S. Atomic Energy Commission. The authors thank H. S. Tessler for performing the experiments.

Index category: Structural Dynamic Analysis.

*Staff Member, Shock Simulation Department.

†Division Supervisor, Shock Simulation Department. Associate Fellow AIAA.

50,000 g accelerometer was mounted on the inner ring surface to sense acceleration in the radial direction. The impulse loading on the outside surface was a radially directed short-duration half-cosine pressure pulse; i.e., pressure varying as cosine θ for $|\theta| < 90°$. Measured radial acceleration was compared with a theoretical prediction as derived in the Appendix.

Experimental Arrangement

The setup is shown schematically in Fig. 1. The ring was 6061-T6 aluminum, o.d. 304.8 mm, 5.1 mm thick, and 50.8 mm wide. Thin aluminum conductors and insulation were assembled on a foam backup mass so that the inside radius of the top conductor (the flyer) was equal to the outside radius of the ring. At switch closure, the capacitor bank discharged and repulsion between conductors propelled the flyer against the ring. Conductor shape[1,2] and initial flyer-to-ring spacing were adjusted to achieve, respectively, half-cosine flyer velocity distribution and simultaneous impact on the ring surface.

An Endevco 2264A-50KR, 50,000 g undamped piezoresistive accelerometer, having full-scale output 500 mv and resonant frequency about 200 kHz was used. The accelerometer, 13 mm square and 5 mm high, weighing 2 g, was pressed into a drop of a quick-setting polysulfide adhesive on the inner surface of the ring. The adhesive cured to form a soft rubber mounting pad of thickness varying 0.05-0.20 mm.

As a measure of rigid body momentum, flight of the ring after flyer impact was recorded by time lapse photographs.[2] Theoretical acceleration response for the impulse level corresponding to the measured rigid body momentum could then be compared with the accelerometer signal.

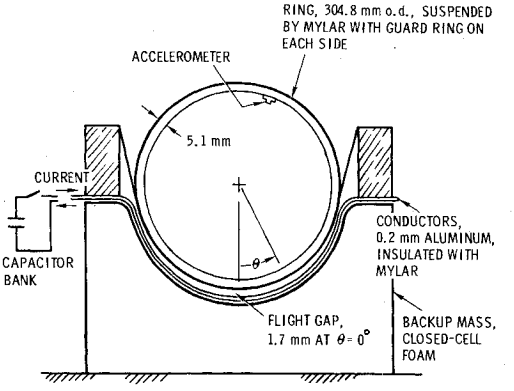

Fig. 1 Experimental arrangement.

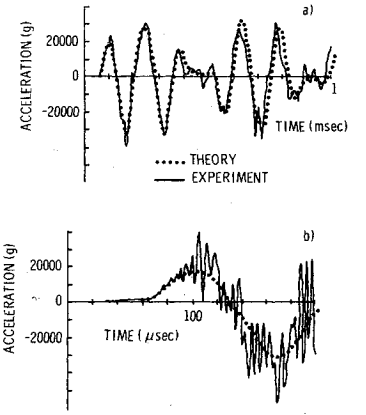

Fig. 2 Comparison of predicted and measured acceleration (positive radially outward); $\theta = 160°$, $I = 201$ Pa. sec.

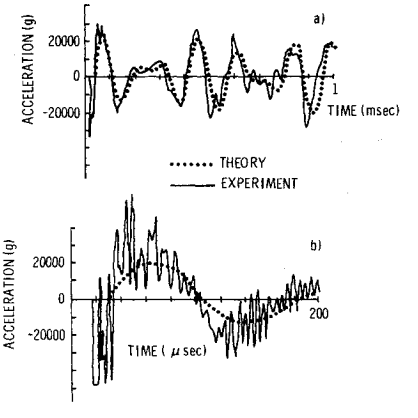

Fig. 3 Comparison of predicted and measured acceleration (positive radially outward); $\theta = 45°$, $I = 152$ Pa·sec.

Results

In Figs. 2 and 3, typical accelerometer records are compared with scaled theoretical predictions. Development of the theoretical predictions is outlined in the Appendix; for this problem, response is dominated by the first three extensional (membrane) modes. The records in Figs. 2a and 3a were electronically filtered (—3 db at 30 kHz). Portions of the same records are shown unfiltered in Figs. 2b and 3b. In the latter, the accelerometer resonant frequency appears superimposed on the radial acceleration of the ring. The large initial negative pulse on the records in Fig. 3 corresponds to flyer impact. This feature is missing from the predicted signal because the calculation is begun after the ring cross section is given an initial velocity distribution appropriate to the theoretical half-cosine impulse load. These results imply that, using an accelerometer of adequate information bandwidth, credible acceleration measurements can be made on an impulse-loaded structure or internal components.

Appendix: Ring Acceleration Response

Solutions for the displacements[2] and stresses[3] in circular elastic rings subjected to a half-cosine impulse load are published. Expressions for the displacement components consist of terms corresponding to purely extensional (membrane) and inextensional (bending) motions. Differentiation of the series displacement expressions to obtain acceleration indicates that the amplitudes of the modes for large wave numbers behave as n^{-3} for the extensional terms and approach a constant for the inextensional terms. The convergence problem in the inextensional series is due to inadequacies in the elementary ring theory. With an improved ring theory[4] which includes the effects of shear deformation and rotatory inertia, the modal amplitudes for the inextensional acceleration behave as n^{-1} for large wave number and convergence problems are avoided. The radial acceleration is given by

$$(\partial^2 w/\partial t^2) = (\partial^2 w_e/\partial t^2) + (\partial^2 w_i/\partial t^2) \qquad \text{(A1)}$$

where w_e and q_i are the extensional and inextensional radial displacement components, measured positive inward, and

$$\frac{\partial^2 w_e}{\partial t^2} = \frac{-Ic}{\rho ha}\left\{\frac{1}{\pi}\sin\tau + \frac{1}{2(2)^{1/2}}\sin[(2)^{1/2}\tau]\cos\theta - \frac{2}{\pi}\sum_{n=2,4}^{\infty}\frac{(-1)^{n/2}\cos n\theta}{(n^2-1)(n^2+1)^{1/2}}\sin[(n^2+1)^{1/2}\tau]^{1/2}\tau]\right\} \qquad \text{(A2)}$$

$$\frac{\partial^2 w_i}{\partial t^2} = \frac{2Ic}{\pi\rho ha}\sum_{n=2,4}^{\infty}\frac{(-1)^{n/2}n^2\cos n\theta}{(n^4-1)\Delta}\left[\omega_1(n^2+1/\alpha^2\beta^2-\omega_1{}^2)\sin\omega_1\tau - \omega_2(n^2+1/\alpha^2\beta^2-\omega_2{}^2)\sin\omega_2\tau\right] \qquad \text{(A3)}$$

in which

$$\Delta^2 = \frac{(n^2-1)^4}{\beta^4(n^2+1)^2} - \frac{2(n^2-1)^2}{\beta^2(n^2+1)}(n^2-1/\alpha^2\beta^2)$$

$$+(n^2+1/\alpha^2\beta^2)^2 2\omega_{1,2}^2 = \frac{(n^2-1)^2}{\beta^2(n^2+1)} + n^2+1/\alpha^2\beta^2 \mp \Delta$$

$$\tau = ct/a,\ c^2 = E/\rho,\ \alpha^2 = h^2/12a^2,\ \beta^2 = E/kG$$

where E, G, and ρ are Young's modulus, shear modulus, and density; h and a are shell thickness and mean radius; t is time; k is the shear deflection coefficient taken as $k=5/6$; g is the acceleration due to gravity; and I is the peak intensity of impulse cosine distributed over $|\theta| < 90°$.

References

[1] Bealing, R., "Impulse Loading of Circular Rings," *Experimental Mechanics, Proceedings of the 11th Annual Symposium*, University of New Mexico, Albuquerque, N. Mex., 1971, pp. 15-26.

[2] Forrestal, M. J. and Overmier, D.K., "An Experiment on an Impulse Loaded Elastic Ring," *AIAA Journal*, Vol. 12, May 1974, pp. 722-724.

[3] Forrestal, M. J., Sagartz, M. J., and Walling, H. C., "Comment on Dynamic Response of a Cylinder to a Side Pressure Pulse," *AIAA Journal*, Vol. 11, Sept. 1973, pp. 1355-1356.

[4] Keer, L. M., Fleming, J. F., and Herrmann, G., "Transient Response of an Elastic Shell in Plane Strain," *The Journal of the Acoustical Society of America*, Vol. 41, No. 2, Feb. 1967, pp. 358-368.

Cylindrical Electrostatic Probes at Angles of Incidence

C. Bruce* and L. Talbot†
University of California, Berkeley, Calif.

Nomenclature

e = charge on electron
k = Boltzman constant
n^i = ion number density, cm^{-3}
p = pressure, torr
r_p = probe radius, cm
T = temperature
T^e = electron temperature
V_p = probe potential, volts
λ_D = Debye length, cm
$\lambda_{\alpha\beta}$ = mean free path for species α and β

Subscripts

∞ = refers to property of freestream
0 = refers to stagnation value

Introduction

In the course of an investigation of conical electrostatic probes[1] it was important to give detailed examination to the current-voltage characteristics of cylindrical probes aligned with, and at angles of incidence to weakly ionized flows, since cylindrical probes were used to measure the charged-particle properties of the flows. The interest in cylindrical probe response stems from the fact that it has been found that the ion current collected by cylindrical probes sometimes exhibits a peak in the neighborhood of zero incidence, apparently for two quite different reasons. One cause of a current peak is the end effect identified by Bettinger and Chen[2] and Hester and Sonin,[3] which is associated with a non-negligible contribution to the probe current from the end of the sheath facing the flow and is characterized by large values of λ_D/r_p. Another explanation which has been suggested for a current peak is that it is due to ion-ion collisions, which inhibit curved trajectory motions of the ions and cause them to move toward the probe in a more-or-less radial fashion. This situation would, of course, be obtained in quite a different range of probe operation than that for which the end effect was significant. Since it was possible to operate the cylindrical probe over a wide range of values of λ_{ii}/r_p, an examination of the effect of ion-ion collisions on probe response was deemed worthwile.

Received January 20, 1975. This research was supported by the Air Force Office of Scientific Research.

Index categories: Plasma Dynamics and MHD; Atomic, Molecular and Plasma Properties.

*Research Assistant; presently Staff Member, MIT Lincoln Laboratory, Lexington, Massachusetts. Member AIAA.

†Professor. Member AIAA.

Experimental Equipment

After ionization in a radio frequency induction heated torch, the test gas (argon) expanded through a converging-diverging nozzle with throat diameter 2.54 cm. The 1.22 m diam test section was maintained at low pressure by three stages of mechanical pumping and two oil booster pumps. Deionization of the flow by surface recombination was employed to vary the ion density by several orders of magnitude. Tantalum honeycombs 0.5 cm long were placed in a chamber which was added to the flow path between the torch exit and the nozzle. Electrons and ions in the flow diffuse to the metal surfaces of the honeycombs where the recombination occurs. The ion density of the flow could be lowered from about 10^{13} to less than 10^9 cm^{-3} by adding up to six of the honeycombs.

A device for varying the angle of incidence of a cylindrical electrostatic probe was built. Mounted on a traverse mechanism, it allowed the probe to be rotated from outside the chamber in such a fashion that the midpoint of the probe collecting surface was the center of rotation. An indicator on the device displayed the angle of incidence to the nearest 0.9° over a range from -90° to +90°. The cylindrical electrostatic probe was made from 0.038 cm diam tungsten wire with an exposed surface length of 0.749 cm. A 45 v battery pack supplied the probe voltage. Two electrometers connected to an x-y recorder measured the probe current-voltage characteristics.

Flow Calibration

The flow region used for the angle of incidence measurements was the exit of the diverging nozzle. The neutral flow properties at that point were determined from stagnation and impact pressure measurements together with stagnation temperature measurements by assuming an ideal gas with isentropic expansion through the nozzle and using the tables of Mueller.[4] The seven different flow conditions, characterized by the number of tantalum honeycomb sections (0-6) placed in the deionization chamber, are listed in Table 1. The electron temperatures for the two highest ion density conditions were measured with a double cylindrical probe using the method of Johnson and Malter.[5]

While the effects of ion-neutral collisions were negligible on the electron temperature measurements, they were important in the single probe measurements of ion densities. To account for these effects we used the mixing formula of Thornton[6] to calculate the ion densities from the measured single probe ion currents. For lower values of ion density, the theory of Laframboise[7] as presented by Sonin[8] was used to determine the collisionless current required by the Thornton formula. But at the highest ion density (no honeycomb) the cold ion theory of Allen, Boyd, and Reynolds[9] as applied to the cylinder by Chen[10] was used to calculate the collisionless current. We now believe that although λ_{in}/r_p may be large, when $(\lambda_{ii}/r_p) \ll 1$, the aligned probe current increases from that predicted by Laframboise to that predicted by Chen. We